Dynamics of diamagnetic Zeeman states ionized by half-cycle pulses

C. Rangan, K. J. Schafer,* and A. R. P. Rau
Department of Physics and Astronomy, Louisiana State University, Baton Rouge, Louisiana 70803
(Received 9 August 1999; published 18 April 2000)

We study the dynamical evolution of diamagnetic Zeeman states in hydrogen and sodium atoms ionized by half-cycle pulses. The eigenstates of the combined Coulomb-diamagnetic potential are determined by solving the Schrödinger equation using a grid-based pseudopotential method. We study states with principal quantum number n between $15-20$ in the l-mixing regime at a magnetic field of 6 T. Diamagnetic states that are initially localized parallel and perpendicular to the magnetic field are subjected to the electric field of a half-cycle pulse (HCP) and their time evolution is monitored. We calculate the total ionized fraction, and also the spectrum of the ionized photoelectrons, keeping the total momentum transferred by the HCP constant and varying the HCP width. We find differences in both the amount of ionization and the form of the photoelectron spectrum for the two classes of localized states. In the impulsive limit, where the width of the pulse is much smaller than typical time scales in the system, the differences are due to the different initial momentum distributions of the parallel and perpendicular states. For longer pulse widths, we find that ionization is supressed as compared with the impulsive limit. The states localized perpendicular to the magnetic field are found to be much more sensitive to the HCP width than the parallel states, which reflects the fact that the two classes of states interact with different parts of the diamagnetic potential during the HCP.

PACS number(s): 32.60.+i, 32.80.Rm

I. INTRODUCTION

Diamagnetic effects for an atom in a magnetic field have been of interest since the first observations of the diamagnetic spectrum in 1939 [1] and, later, of the quasi-Landau spectrum in 1969 [2]. The study of the energy levels of hydrogen as a function of magnetic field strength [3] led to the discovery of approximate symmetries [4] at low magnetic fields and energies (corresponding to low principal quantum number n). Since then, while experimental and theoretical studies have led to greater understanding of Coulomb diamagnetism [5], it remains a fundamental problem that is the subject of much current research [6].

An atom in a strong magnetic field is an example of a system that exhibits competing symmetries (spherical symmetry due to the Coulomb potential and cylindrical symmetry due to the magnetic field). It is not separable in any coordinate system, in contrast to its counterpart, an atom in an electric field, which separates in parabolic coordinates. At low fields and energies (the ''l-mixing'' regime), the diamagnetic eigenstates are divided into two classes, both showing strong spatial localization (parallel and perpendicular to the magnetic field) [7]. This type of localization is known to be a general feature of perturbed degenerate systems with competing symmetries [8]. Previous results [7] have successfully explained the principal static features of the l-mixing regime (such as the spatial localization, angular momentum distribution in the eigenstates, and the energy eigenvalues), as well as the near-threshold quasi-Landau region [5]. So the spectroscopy of these states is well understood. At higher energies and magnetic fields, a complex structure is seen in the spectrum, some of which can be explained by trajectories in the chaotic region of the classical diamagnetic Kepler problem [9]. Statistical distributions of energy level spacings in hydrogen show a change in nearest-neighbor spacings from Poisson to Wigner, corresponding roughly to the change in the classical dynamics from quasi-integrable (at low energies and magnetic fields) to chaotic (at high energies or magnetic fields) [10]. In nonhydrogenic atoms, scattering from the ion core can be expected to play a large role that may be investigated by studying the dynamics of Rydberg wave packets in strong magnetic fields [11].

The motivation for our study is the recent development of a new spectroscopic method for studying the dynamics of Rydberg atoms—their ionization using nearly unipolar electromagnetic pulses. These are referred to as ''half-cycle pulses'' (HCPs) [12] since their electric field lies almost completely in one half of the optical cycle. In traditional spectroscopic methods like photoionization, an electron is ionized only when it is near the atomic core, which is needed to absorb the recoil momentum. Therefore, the ionization characteristics reflect the state of the atom for only the very short time when the electron is near the atomic core. An HCP, by contrast, can contribute linear momentum and thus ionize an electron anywhere along its trajectory [13]. HCPs have been used to study the ionization of Rydberg eigenstates, Stark states, and Rydberg wave packets away from the core [13]. They have also been used to create wave packets [14]. If the pulse width of the HCP is much smaller than the characteristic time scale of the quantum state being studied (for example, the Kepler orbital period for a radial wave packet), then time-delay spectroscopy can be performed [13]. Recently, this technique has been used to study the ionization of Stark states, showing an asymmetry in the ionization probability depending on the localization of the states that are ionized [15,16]. Since the diamagnetic system is also characterized by localization of states (parallel and perpendicular to the magnetic field), ionization by HCPs may be

*Corresponding author.

expected to yield rich and interesting results in this system as well.

In this paper, we show that the HCP ionization of diamagnetic Zeeman states depends strongly on their spatial localization. Our theoretical methods permit not only the accurate calculation of the known static properties, but also a study of the dynamics of these states under the influence of a time-dependent external field. The technique facilitates the study of different alkali atoms and the results (ionization vs the HCP width, for example) are presented in a manner that they can be explored immediately by an experiment.

Eigenstates of the Coulomb-diamagnetic Hamiltonian

The Hamiltonian for an electron in the combined potential due to the Coulomb field of the nucleus and an external static magnetic field **B** in the $\hat{\mathbf{z}}$ direction, is given by [17]

$$H=\frac{\mathbf{P}^2}{2}-\frac{1}{r}+A(r)\mathbf{L}\cdot\mathbf{S}+\frac{\mathbf{L}\cdot\mathbf{B}}{2}+\mathbf{S}\cdot\mathbf{B}+\frac{\mathbf{B}^2}{8}(x^2+y^2). \quad (1)$$

We use atomic units throughout ($\hbar=m_e=e=1$, one atomic unit of magnetic field $=2.35\times10^5$ T). The decoupling of the spin and angular momentum takes place at very low values of the magnetic field, so that the contribution of spin may be ignored. The paramagnetic term, which is linear in **B**, adds a constant energy to the Hamiltonian, yielding an overall phase factor in the time-dependent wave function, and may also be ignored. This Hamiltonian also conserves parity; thus, for the Coulomb-diamagnetic problem, the magnetic quantum number m, as well as parity, are conserved quantities. For each value of m, the unperturbed Hamiltonian is $(n-|m|)$-fold degenerate (where n is the principal quantum number). The degeneracy of the l states, $|m|\leq l<n$, is then lifted by the diamagnetic potential which is quadratic in the magnetic field.

The diamagnetic spectrum is characterized by two regions: low energies and magnetic fields—the l-mixing regime, where the wave functions of the adjacent n manifolds are not mixed; and higher energies or magnetic fields—the n mixing regime, with significant overlap of adjacent n manifolds. In the l-mixing regime, the electron probability densities exhibit strong angular localization [6] as shown in Fig. 1. The lowest energy state of a single n manifold is localized along the direction of the magnetic field in the potential valley, while the highest energy states are localized perpendicular to the magnetic field on a potential ridge as seen in Figs. 1(a) and 1(b), respectively. The highest energy ''ridge'' states are the diamagnetic counterpart of the ''uphill'' states in the Stark system. States with intermediate energies, the ''separatrix'' states shown in Fig. 1(c), are not localized. Both the highest and lowest energy states have dominantly low angular momentum contributions, $l<\sqrt{n}$, and the few separatrix states have all the high angular momenta [8].

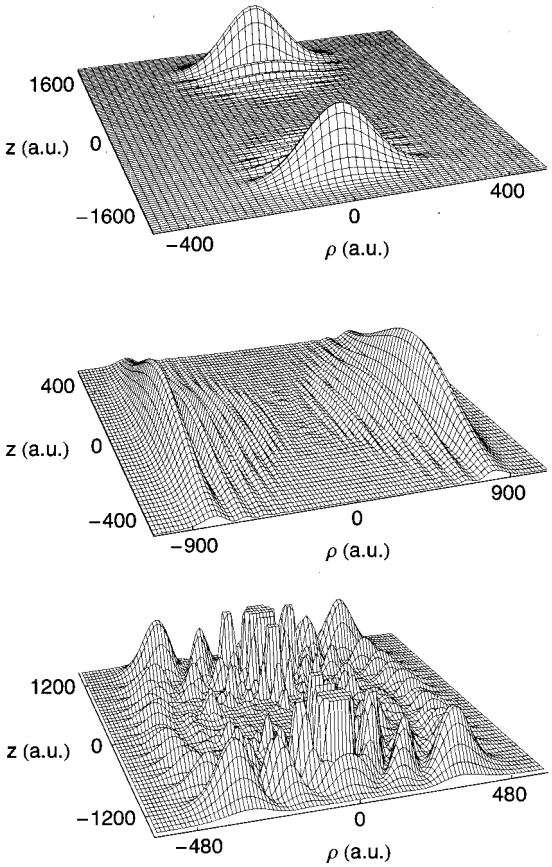

FIG. 1. Electron probability distributions of $n=20$ diamagnetic Zeeman states of hydrogen. $m=0$, even parity, $\mathbf{B}=6T\mathbf{z}$. The lowest energy states (top) are localized in the direction of the magnetic field and the highest energy states (middle) are localized perpendicular to the magnetic field. A nonlocalized state around the separatrix is shown at the bottom. The probability distributions are multiplied by r^2 to aid visibility.

II. CONSTRUCTION OF COULOMB-DIAMAGNETIC EIGENSTATES

We begin by finding the eigenstates of the unperturbed atomic Hamiltonian. The Schrödinger equation for an electron in an unperturbed atom is

$$H_0\Psi(\mathbf{r})=\left[\frac{\nabla^2}{2}+V(\mathbf{r})\right]\Psi(\mathbf{r})=E\Psi(\mathbf{r}). \quad (2)$$

In hydrogen, the potential $V(\mathbf{r})$ is Coulombic, i.e., $V(\mathbf{r})=-1/r$ and the Hamiltonian is separable in spherical coordinates. For alkali metal atoms, we use a nonlocal pseudopotential [18]:

$$V(\mathbf{r})=\sum_l V_l(r)|l\rangle\langle l|+V_{pol}(r)-\frac{1}{r}, \quad (3)$$

where $V_l(r)$ is an l-dependent short-range contribution and $V_{pol}(r)$ is a polarization term. The solution is found by expanding the wave function in a mixed basis of discretized radial functions times spherical harmonics, retaining a finite number of spherical harmonics:

$$\Psi(r_j,\theta,\phi)=\sum_l \Phi_l(r_j)Y_l^m(\theta,\phi), \quad (4)$$

where j is an index corresponding to a radial grid point. The resulting equation for $\Phi_l(r_j)$ is then solved. Following the method in Ref. [19], the numerical solution is found on a nonuniform radial grid. The grid is closely spaced near the nucleus, with the spacing increasing to a constant value towards the outer edge. This makes it possible to represent Rydberg wave functions accurately. Both positive and negative energy states are represented on the same grid, thus allowing us to study the dynamics of bound states as well as ionization problems. The unperturbed eigenstates, which we label as $\Phi_{nl}(r_j)$, are eigenstates of a real, symmetric, tridiagonal matrix.

We next construct the matrix elements of the diamagnetic potential

$$V_B=\frac{\mathbf{B}^2}{8}(x^2+y^2), \tag{5}$$

in a restricted unperturbed basis Φ_{nl} with n ranging from n_{min} to n_{max}. The only nonzero matrix elements are those that connect states of angular momentum l with those of l or $l\pm 2$. Since the total potential conserves parity, we can find odd and even parity states (which contain odd or even l contributions) independently. The diagonalization of the diamagnetic Hamiltonian thus reduces to finding eigenvalues E^k and eigenvectors $|k\rangle$ of a real, symmetric, pentadiagonal matrix. We vary the number of basis states to check the convergence of the energy eigenvalues. Typically, we use a basis of 220 states around $n\simeq 20$. The eigenstates

$$|k\rangle=\sum_l a_l^k(r)|l\rangle, \tag{6}$$

are again products of radial and angular functions; therefore, the dynamics and the symmetry of the problem may be separated easily. Our calculations of the localization of the probability distributions and l contributions to the eigenstates are in excellent agreement with previously published calculations [8].

The excitation and ionization properties of the combined Coulomb-diamagnetic eigenstates $|k\rangle$ may be studied individually by examining the time-dependent dynamics when starting in a single diamagnetic state. It is also possible to make a coherent wave packet by promoting an electron initially in a deeply bound state (that is not affected by the external magnetic field) with a laser pulse to a superposition of higher diamagnetic states. In this paper, we focus on the HCP ionization of the eigenstates. The HCP ionization of wave packets will be treated in a subsequent paper. It may be noted that the HCP itself creates a wave packet when it acts on an eigenstate.

III. IONIZATION BY A HALF CYCLE PULSE

We next examine the ionization of an electron in the combined Coulomb-diamagnetic potential by a half-cycle pulse. The HCP used to ionize the electron is modeled as a time-dependent electric field of the form:

$$\mathbf{E}(t)=\begin{cases}\hat{\mathbf{z}}E_{\mathrm{HCP}}\sin\left(\dfrac{2\pi}{2\tau_{pulse}}t\right), & 0\leqslant t\leqslant\tau_{pulse},\\ 0 & t>\tau_{pulse},\end{cases} \tag{7}$$

where E_{HCP} is the maximum field amplitude in atomic units and τ_{pulse} is 1.5 times the full width at half maximum (FWHM) of the electric field. The momentum transferred by such a pulse to a free electron in the absence of any other interactions is

$$\mathbf{Q}=-\int_0^{\tau_{pulse}}dt\mathbf{E}(t). \tag{8}$$

In the limit that the pulse width is very small, no other interactions are possible during the pulse, and the effect of the HCP is to boost the electron by a momentum $\mathbf{Q}$

$$\Psi_f(\mathbf{r},t)=e^{i\mathbf{Q}\cdot\mathbf{r}}\Psi_i(\mathbf{r},t). \tag{9}$$

This is the impulse approximation of an HCP. We study the excitation and ionization between two limits—when the pulse width is much smaller than typical time scales in the system (the impulse approximation) and when it is so large that the impulse approximation is invalid.

The time evolution of a state in the combined Coulomb-diamagnetic potential under the influence of an HCP is treated by the Peacemann-Rachford method [20]. In the total Hamiltonian $H=H_0+H_I$, H_0 connects adjacent radial points of functions with the same l value, whereas the interaction $H_I=H_B+H_{\mathrm{HCP}}$ couples functions of different l values $(l\rightarrow l,l\pm 1,l\pm 2)$ at the same radial point:

$$\Psi(r,t+\delta t)=e^{-iH\delta t}\Psi(r,t). \tag{10}$$

We expand the propagator as

$$\Psi(r,t+\delta t)=\left[1+iH_0\frac{\delta t}{2}\right]^{-1}\left[1+iH_I\frac{\delta t}{2}\right]^{-1}\left[1-iH_I\frac{\delta t}{2}\right]\times\left[1-iH_0\frac{\delta t}{2}\right]\Psi(r,t). \tag{11}$$

The Peacemann-Rachford propagator agrees with the full propagator up to the third order in δt. The first two operations on $\Psi(r,t)$ are straightforward, the next two require finding the solution to five-term and three-term recurrence relations in l and r, respectively. The computational complexity of this operation is of first order in $N_r\times N_l$. The HCP field exerts a torque on the electron and consequently many higher l values are mixed in during the time evolution. Although our initial state may have only low angular momentum components, we use up to $l\simeq 100$ during the time evolution of a state under the influence of an HCP in the combined Coulomb-diamagnetic potential. Since the commutator $[H_0,H_I]\neq 0$, the Peacemann-Rachford propagator is not unitary. Therefore, the time step δt must be small enough to insure that the higher order terms in the expansion of the exponential in Eq. (10) are negligible. We monitor the norm of the wave function at every time step as a check on this

property. We can perform 120 000 such space-time steps in 1 CPU second on a DEC-alpha workstation.

After an HCP has been applied to an electron initially in an eigenstate $|k\rangle$, the energy spectrum of the ionized photoelectrons is obtained by projecting the final state wave function (at any time after τ_{pulse}) onto the eigenstates of the final state Hamiltonian $H_f = H_0 + H_B$ as in Ref. [21]. The probability of finding an electron of energy E_i in the final state with a resolution of 2γ is

$$P(E_i, H_f) = \left\langle \Psi_f \left| \frac{\gamma^4}{(H_f - E_i)^4 + \gamma^4} \right| \Psi_f \right\rangle. \tag{12}$$

The total ionized fraction is also given by the area under this curve: $\Sigma_i P(E_i)$. Since the applied magnetic field (6 T) is very small compared to the magnetic field that an electron experiences due to its motion in the field of the nucleus (10^5 T), we can simplify this calculation by setting $H_f = H_0$, which makes Eq. (12) separable in r and l. The validity of this approximation is checked by finding $P(E_i, H_f)$, using the method of alternating direction iteration (ADI) [20,22] with the full $H_f = H_0 + H_B$. This method uses the unperturbed photoelectron ionization probability $P(E_i, H_0)$ as a first guess and iteratively determines the final photoelectron ionization probability $P(E_i, H_f)$ to successively higher orders in the perturbation (which is of second order in the magnetic field). The photoelectron ionization probability $P(E_i, H_f)$ differs from the first guess $P(E_i, H_0)$ by a small amount of the order of 10^{-5} and converges rapidly. There is also no discernable change in the photoelectron spectra as compared to those calculated by projecting onto the unperturbed states. To our knowledge, this is the first time that the energy window method has been used with a nonseparable potential.

IV. RESULTS AND DISCUSSION

We begin with hydrogen in a magnetic field of $B = 6$ T ($= 2.55 \times 10^{-5}$ a.u.) along the z direction. The states corresponding to the $n = 20$ ($m = 0$) manifold are within the l-mixing regime. Choosing the lowest energy (valley), highest energy (ridge), and separatrix states of even parity from this manifold, we study their ionization behavior. The ionizing HCP is linearly polarized with its electric field vector in the z direction.

Figure 2 shows the ionized fractions of these three states as a function of the momentum transferred by the HCP in the impulse approximation. For a classical electron of momentum $\mathbf{p}_i$, the final momentum after its interaction with an HCP is $\mathbf{p}_f = \mathbf{p}_i + \mathbf{Q}$, where $\mathbf{Q}$ is the momentum transferred by the HCP. The change in its energy is equal to

$$\begin{aligned} \Delta E &= \frac{\mathbf{p}_f^2}{2} - \frac{\mathbf{p}_i^2}{2} \\ &= \mathbf{p}_i \cdot \mathbf{Q} + \frac{Q^2}{2}. \end{aligned} \tag{13}$$

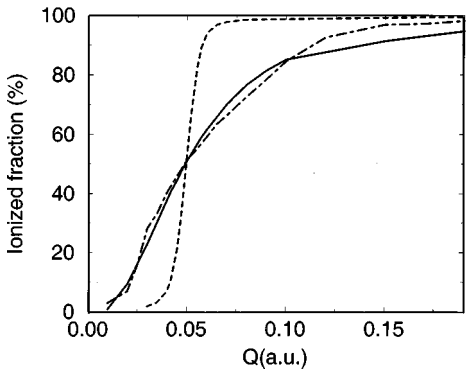

FIG. 2. Calculated ionized fractions of photoelectrons as a function of total momentum transferred (impulse approximation). Solid line: lowest energy state. Dashed line: highest energy state. Dot-dashed line: a separatrix state.

To ionize an electron, this change in energy must exceed the binding energy $|E_b|$. Since the electric field of the HCP is in the z direction, the initial z momentum of an electron that has threshold energy after the pulse is given by

$$p_{0z} = \left(|E_b| - \frac{Q^2}{2} \right) \Big/ Q. \tag{14}$$

The probability that an electron is ionized in this classical impulse approximation is just the probability that its initial momentum in the z direction is greater than p_{0z} [23]. In this approximation, the slope of the curve in Fig. 2 is proportional to the dispersion in the z component of the momentum of the state. If a state has a large z component to its momentum, it does not require much $\mathbf{Q}$ to be ionized and vice versa. The highest energy state has a much steeper threshold than the lowest energy or separatrix states. One can see that the highest energy state, which is localized perpendicular to the magnetic field, has very little momentum in the z direction so that there is little likelihood of ionization for Q less than the threshold value of 0.052 a.u. The dispersion in the z momentum is also very small. The lowest energy and separatrix states have significant probability densities and momenta along the z direction and therefore show similar ionization curves with appreciable ionization even at lower Q.

Figure 3 shows the ionization spectra obtained in the impulse approximation for the three states (ridge, valley, and separatrix) ionized by an HCP. We compare a *soft* kick, which transfers energy just above threshold, and a *hard* kick, which completely ionizes the Rydberg electron. At threshold, only those parts of the electron probability distribution that have positive z momentum get ionized. The distribution for the soft kick is therefore peaked at zero energy. For a hard kick, the spectra are symmetric and peaked at the energy corresponding to $Q^2/2 - |E_b|$, where E_b is the energy of the bound state. From the discussion in the previous paragraph, this implies that the average z momentum is equal to zero. Such a feature is also seen in the total ionization cross section for charged particle collisions that are peaked about the energy-momentum conserving value [24]. The ionization of an electron by an HCP, an electromagnetic pulse, shows

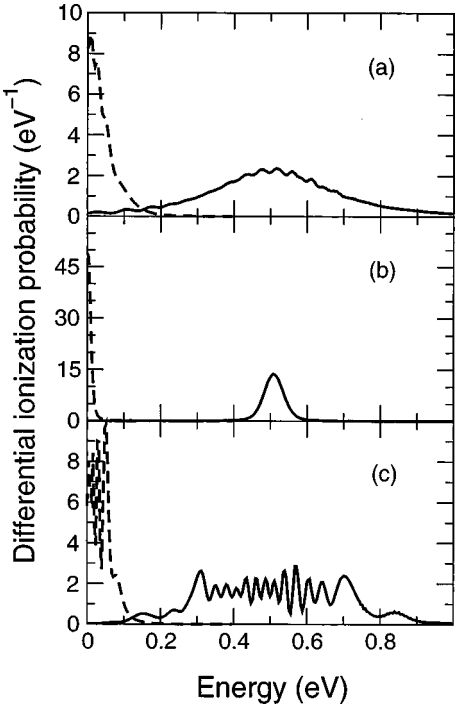

FIG. 3. Calculated differential ionization probabilities of diamagnetic Zeeman states of hydrogen ionized by an HCP (impulse approximation) as a function of photoelectron energy for (a) lowest, (b) highest, and (c) separatrix states. Solid line: *hard* kick, $Q=0.2$ a.u. Dashed line: *soft* kick, $Q=0.052$ a.u. The area under the curve yields the total ionized fraction.

characteristics of collisional ionization by charged particles when the pulse width of the HCP is very small (the impulsive limit). The spectrum of the lowest energy state in Fig. 3(a) shows an oscillatory structure corresponding to the two possible *z*-momentum directions—along and opposite the HCP field. The highest energy state [Fig. 3(b)], which has very little *z* momentum, does not show this structure. The separatrix state seen in Fig. 3(c) shows a complex structure in its spectrum.

In Fig. 4, we study the ionized fractions of the lowest, highest, and separatrix $n=20$ states as a function of the width of the HCP while keeping the total impulse Q constant. Q is chosen to be 0.052 a.u. such that the energy $Q^2/2-|E_b|$ is just above threshold. In all three cases, the ionization is suppressed as the HCP width becomes comparable to the Kepler period ($2\pi n^3 \simeq 1.2$ ps). Clearly, the nature of this decrease in ionization depends on the localization of the state. The lowest energy states, localized in the direction of the magnetic field, show a sharp suppression of ionization when the HCP width becomes approximately equal to one-half of the Kepler period. The highest energy states, localized perpendicular to the magnetic field, show a smooth decrease in ionization with increasing pulse width and are the most sensitive to deviation from the impulsive limit. The separatrix states show the least loss of ionization. This supression of ionization by using longer HCPs is in contrast to optical ionization where ionization of Rydberg atoms is suppressed by using shorter laser pulses [25]. The photoelectron spectra at $\tau_{pulse}=0$, $\tau_{Kepler}/2$, and τ_{Kepler} seen in Fig. 5

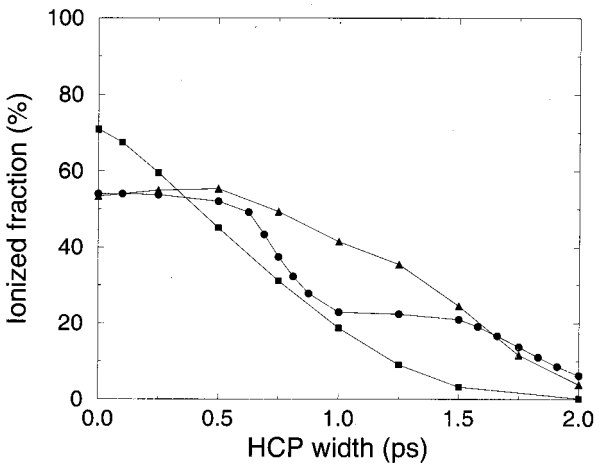

FIG. 4. Effect of width of HCP on ionization of $n=20$ diamagnetic states (circles, lowest; squares, highest; triangles, separatrix). The total momentum transferred Q is kept constant at 0.052 a.u.

show that the energy gained by the photoelectron decreases as the pulse width is increased, thus decreasing the ionized fraction. We now discuss the dynamics of this ''energy loss'' as a function of pulse width.

In the impulse approximation, the electron does not have time to move during the pulse and interacts only with the electromagnetic field of the HCP. In the opposite limit, when the pulse width is long, the electron may interact with the ion core and the diamagnetic potential, as well as the electromagnetic field during ionization. The change in energy of an electron due to the HCP (treating the electron as a classical particle) is given by

$$\Delta E = -\int_0^{\tau_{pulse}} dt\, \mathbf{v}\cdot\mathbf{E}_{\mathrm{HCP}}, \tag{15}$$

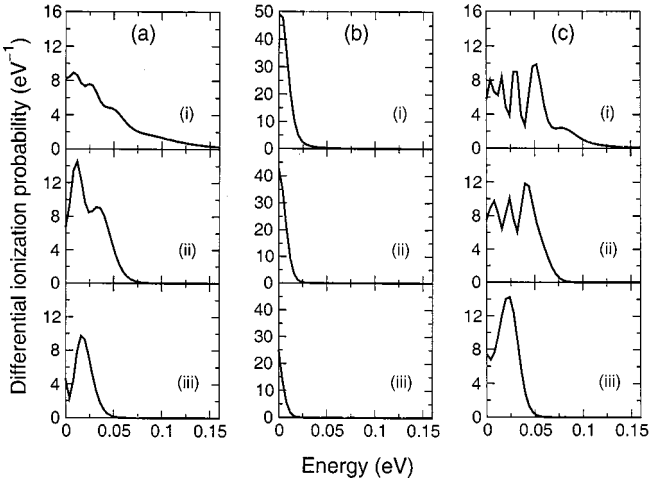

FIG. 5. Photoelectron spectra of $n=20$ diamagnetic states when the HCP width is (i) 0 (impulse approximation), (ii) $\tau_{Kepler}/2$, (iii) τ_{Kepler} for (a) lowest, (b) highest, and (c) separatrix states, respectively. The decrease in the total ionized fraction is accompanied by a smaller photoelectron energy.

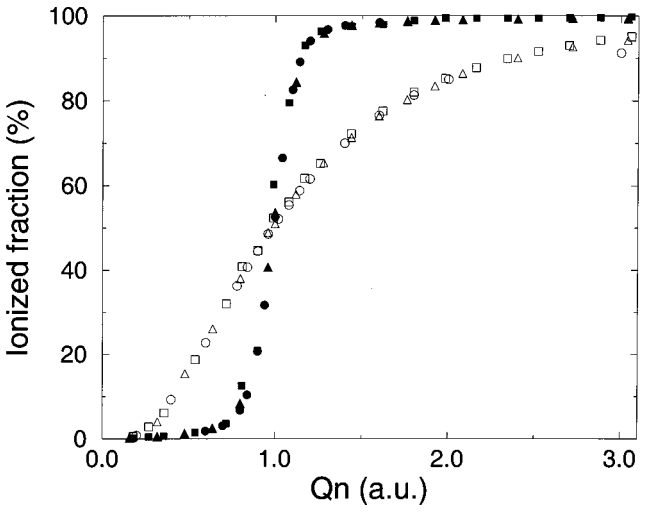

FIG. 6. Ionization curves in the impulse approximation as a function of the total momentum transferred times n for diamagnetic states of hydrogen: $n=20$ (circles), $n=18$ (squares), and $n=16$ (triangles). Open points: lowest energy states. Filled points: highest energy states.

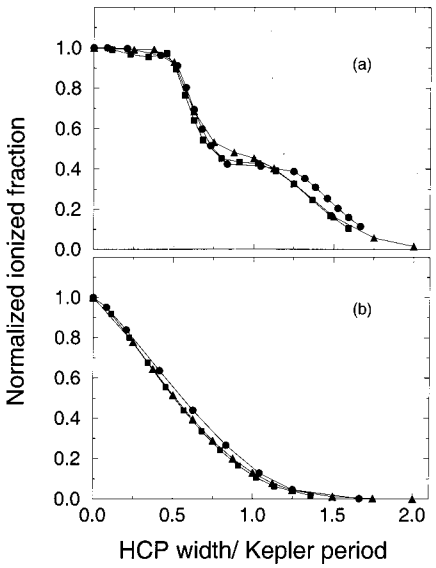

FIG. 7. Plot of ratio of ionized fraction at finite HCP width to that in the impulse approximation for the same momentum transferred vs the ratio of HCP width to the Kepler orbital period $2\pi n^3$. $n=20$ (circles), $n=18$ (squares), and $n=16$ (triangles); (a) lowest, (b) highest energy states.

where **v** is the velocity of the electron. When interacting with the ion core, the electron changes its direction of motion thus gaining less net energy than it would have otherwise. The ionization dynamics may be expected, therefore, to show a dependence on the pulse width of the HCP at time scales corresponding to the interaction of the electron with the ion core, that is, the Kepler orbital period. The lowest energy state is localized along the direction of the magnetic field and can interact with the ion core on a time scale of one half the Kepler period [since the initial electron probability distribution is peaked near the classical turning point as seen in Fig. 1(a)]. This is reflected in the sudden drop in the ionized fraction as $\tau_{pulse}\sim\tau_{Kepler}/2$. The highest energy states are localized perpendicular to the magnetic field and interact differently with the core. The separatrix states do not lose as much energy as the lowest or highest energy states.

These results may be understood better by studying the localized states of different manifolds. Figure 6 shows calculations performed for three manifolds, $n=20$, 18, 16, at $B=6$ T. This is still within the l-mixing regime. The ionization probability (in the impulsive limit) as a function of Qn, the product of the momentum imparted by the HCP and the principal quantum number (the classically scaled momentum), is seen to be universal for the states of the same localization. Figure 7 shows the ratio of the ionized fraction at a finite HCP width to that in the impulse approximation for threshold Q plotted against the ratio of the HCP width to the classical Kepler period $\tau_{Kepler}\simeq 2\pi n^3$ for both the lowest and highest states. These are also calculated for $n=16$, 18, and 20, with Kepler periods of ~ 0.6 ps, 0.9 ps, and 1.2 ps, respectively, ionized by pulses with Q values corresponding approximately to the threshold energies of the states. The curves lie on top of each other, indicating that the Kepler orbital period is a significant time scale for each of these localized states. The drop in the ionization probability of the lowest energy states at approximately $\tau_{Kepler}/2$ is steeper as the value of n increases. This suggests that as n increases, the system approaches classical behavior wherein an electron starting from a point in the orbit furthest from the ion core (i.e., near the classical turning point) can interact with the core at times $\tau_{Kepler}/2$ and again at $3\tau_{Kepler}/2$.

We have repeated many of the hydrogen calculations using a pseudopotential appropriate for describing valence orbitals in sodium. In sodium, the quantum defect in the s and p channels causes two states, one of s character and one of p character, to split off in energy from the rest of the unperturbed hydrogenic states of a single n manifold. When a magnetic field of $B=6T$ is applied, these degenerate states do not contain significant contributions from the $l=0$ or $l=1$ angular momenta but retain all the other features just as in hydrogen. We choose the lowest energy, separatrix, and highest energy states of the remaining $n=20$, $m=0$ even parity manifold and the s split-off state nearest in energy. When ionized by an HCP in the impulsive limit, the highest, lowest, and separatrix states of the $n=20$ manifold show the same behavior as in hydrogen, as shown in Fig. 8. The nearest s split-off state, which has mainly $l=0$ character, shows significantly different behavior. Its photoelectron spectrum is also very different from that of the localized diamagnetic states as shown in Fig. 9. But, for the localized states, the quantum defect does not change the HCP ionization characteristics qualitatively.

V. CONCLUSIONS

In summary, we have presented an efficient theoretical technique for studying the dynamical evolution of atomic systems in external fields. We have shown that the HCP ionization dynamics of Zeeman states in the l-mixing regime depends strongly on the localization of the initial diamag-

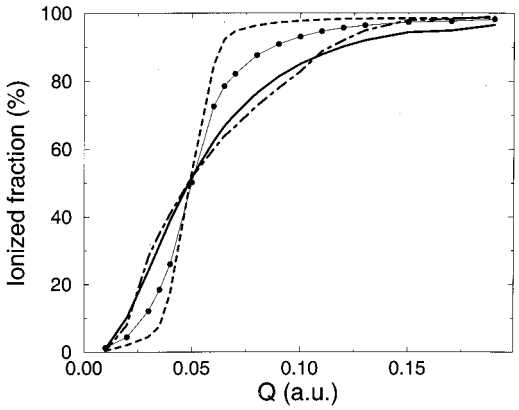

FIG. 8. Calculated ionized fractions of photoelectrons as a function of total momentum transferred (impulse approximation) in $n \simeq 20$, $m=0$, even parity diamagnetic states of sodium. Solid line: lowest energy state. Dashed line: highest energy state. Dot-dashed line: separatrix state. Filled circles: *s* split-off state.

netic state. In the limit of very short HCPs ($\tau_{pulse} \ll \tau_{Kepler}$), the determination of the ionized fraction as a function of the momentum transferred by the pulse is a direct measure of the *z* momentum of these states.

As the width of the HCP increases (keeping the total momentum transferred a constant), the ionization of the diamagnetic states is suppressed. The decrease in ionization is also accompanied by a decrease in the energy gained by the Rydberg electron during ionization, as seen in the calculated photoelectron spectra. The decrease in the ionization fraction is also sensitive to the localization of the initial states. We find that the states that are localized perpendicular to the magnetic field are more sensitive to the increase in HCP width than the states localized parallel to the magnetic field.

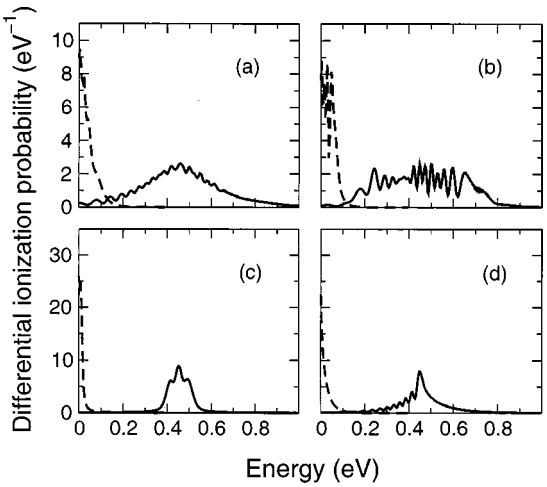

FIG. 9. Calculated ionization spectra of diamagnetic states in sodium ionized by HCP (impulse approximation) for (a) lowest, (b) separatrix, (c) highest, and (d) *s* split-off states. Solid line: *hard* kick, $Q=0.19$ a.u. Long-dashed line: *soft* kick, $Q=0.05$ a.u.

This effect is understood only qualitatively at present.

Similarities in the HCP ionization of localized diamagnetic states in hydrogen and sodium point to the features of ionization being a general characteristic of localized diamagnetic states of atoms in the *l*-mixing regime. These measurements may be made at reasonable laboratory magnetic fields. Indeed, our preliminary results have prompted plans for such experiments that will soon be underway [26].

ACKNOWLEDGMENTS

It is a pleasure to acknowledge helpful comments from L. D. Noordam and A. Guertler. We acknowledge support from the National Science Foundation Grant No. PHY-9733890.

[1] F.A. Jenkins and E. Segre, Phys. Rev. **55**, 52 (1939).

[2] W.R.S. Garton and F.S. Tomkins, Astrophys. J. **158**, 839 (1969).

[3] M.L. Zimmerman, J.C. Castro, and D. Kleppner, Phys. Rev. Lett. **40**, 1083 (1978); M.L. Zimmerman, M.M. Kash, and D. Kleppner, *ibid.* **45**, 1092 (1980).

[4] E. Solov'ev, Pis'ma Zh. Eksp. Teor. Fiz. **34**, 278 (1981) [JETP Lett. **34**, 265 (1981)]; C.W. Clark, Phys. Rev. A **24**, 605 (1981); D. Delande and J.C. Gay, Phys. Lett. **82A**, 393 (1981); D. Herrick, Phys. Rev. A **26**, 323 (1982); J. Gay, D. Delande, F. Biraben, and F. Penant, J. Phys. B **16**, L693 (1983).

[5] A.R.P. Rau, Comments At. Mol. Phys. **10**, 19 (1980); J. Main, G. Weibusch, A. Holle, and K.H. Welge, Phys. Rev. Lett. **57**, 2789 (1986); D. Wintgen and H. Friedrich, J. Phys. B **19**, 1261 (1986); G.R. Welch *et al.*, Phys. Rev. Lett. **62**, 1975 (1989); C. Iu *et al.*, *ibid.* **63**, 1133 (1989); **66**, 145 (1991); P.F. O'Mahony and F. Mota Furtado, *ibid.* **67**, 2283 (1991); D. Delande and K.T. Taylor, J. Phys. B **25**, L525 (1992); **26**, 1775 (1993); D. Delande *et al.*, *ibid.* **27**, 2771 (1994); P. Dando *et al.*, Phys. Rev. Lett. **74**, 1099 (1995).

[6] J. Rao and K.T. Taylor, J. Phys. B **30**, 3627 (1997); J.P. Connerade *et al.*, *ibid.* **30**, 3627 (1997); A.R.P. Rau and G.B. Armen (to be published).

[7] A.R.P. Rau, Phys. Rev. A **16**, 613 (1977); U. Fano, F. Robicheaux, and A.R.P. Rau, Phys. Rev. A **37**, 3655 (1988); A.R.P. Rau, Phys. Rev. Lett. **63**, 244 (1989); P.A. Braun, Rev. Mod. Phys. **65**, 115 (1993).

[8] A.R.P. Rau, in *Aspects of Electron Melecule Scattering and Photoionization*, edited by A. Herzenberg, AIP Conf. Proc. No. 204 (AIP, New York, 1990), p. 24; J. Phys. B **27**, 2719 (1994).

[9] D. Wintgen and H. Friedrich, J. Phys. B **19**, L99 (1986); **19**, 991 (1986); Phys. Rev. Lett. **57**, 571 (1986); Phys. Rev. A **35**, 1464 (1987); A. Holle *et al.*, Z. Phys. D: At., Mol. Clusters **5**, 279 (1987); Phys. Rev. Lett. **61**, 161 (1988); M.L. Du and J.B. Delos, Phys. Rev. A **38**, 1896 (1988); **38**, 1913 (1988).

[10] D. Delande and J.C. Gay, Phys. Rev. Lett. **57**, 2006 (1986); J. Zakrzewski, K. Dupret, and D. Delande, *ibid.* **74**, 522 (1995); T. Jonckheere, B. Grémaud, and D. Delande, *ibid.* **81**, 2442 (1998).

[11] J. Wals *et al.*, Phys. Rev. Lett. **72**, 3783 (1994); W. Schweizer and W. Jans, Phys. Rev. A **57**, 1186 (1998).

[12] R.R. Jones, D. You, and P.H. Bucksbaum, Phys. Rev. Lett. **70**, 1236 (1993); C.O. Reinhold, M. Meller, H. Shao, and J. Burgdorfer, J. Phys. B **26**, L659 (1993); N.E. Tiekling, T.J. Bensky, and R.R. Jones, Phys. Rev. A **51**, 3370 (1995); M.T. Frey, F.B. Dunning, C.O. Reinhold, and J. Burgdorfer, *ibid.* **53**, R2929 (1996).

[13] C. Raman, T.C. Weinacht, and P.H. Bucksbaum, Phys. Rev. A **55**, R3995 (1997); C. Raman, C.W.S. Conover, C.I. Sukenik, and P.H. Bucksbaum, Phys. Rev. Lett. **76**, 2436 (1996).

[14] M.B. Campbell, T.J. Bensky, and R.R. Jones, Phys. Rev. A **59**, R4117 (1999), and references therein.

[15] R.R. Jones *et al.*, Phys. Rev. A **51**, R2687 (1995).

[16] A. Bugacov, B. Piraux, M. Pont, and R. Shakeshaft, Phys. Rev. A **51**, 4877 (1995); C.O. Reinhold *et al.*, J. Phys. B **28**, L457 (1995).

[17] T.F. Gallagher, *Rydberg Atoms* (Cambridge University Press, Cambridge, England, 1994).

[18] J.N. Bardsley, *Case Studies in Atomic Physics* (North-Holland, Amsterdam, 1974), Vol. 4, p. 302.

[19] J.L. Krause and K.J. Schafer, J. Phys. Chem. A **103**, 10 118 (1999).

[20] R. Varga, *Matrix Iterative Analysis* (Prentice-Hall, Englewood Cliffs, NJ, 1963).

[21] K.J. Schafer, Comput. Phys. Commun. **63**, 427 (1991).

[22] S. E. Koonin, *Computational Physics* (Benjamin Cummings, New York, 1986), p. 170.

[23] R.R. Jones, Phys. Rev. Lett. **76**, 3927 (1996).

[24] U. Fano and A.R.P. Rau, *Atomic Collisions and Spectra* (Academic, Orlando, 1986), Chap. 3, pp. 50–52.

[25] J.H. Hoogenraad, R.B. Vrijen, and L.D. Noordam, Phys. Rev. A **50**, 4133 (1994).

[26] L.D. Noordam and A. Guertler (private communication).